Mechanical properties and high temperature oxidation resistance of (AlCrTiV)N coatings synthesized by cathodic arc deposition

Mathieu Nussbaum, Mohammad Arab Pour Yazdi, Alexandre Michau, Eric Monsifrot, Frederic Schuster, Hicham Maskrot, Alain Billard

Mechanical properties and high temperature oxidation resistance of (AlCrTiV)N coatings synthesized by cathodic arc deposition

M. Nussbaum[a,b,*], M. Arab Pour Yazdi[c], A. Michau[d], E. Monsifrot[b], F. Schuster[e], H. Maskrot[d], A. Billard[c]

[a] *Université Paris-Saclay, Ecole Doctorale 2MIB, pôle Chimie Inorganique et Matériaux, Bât.350, 91400, Orsay, France.*

[b] *Dephis, 74 rue Armand Japy, 25460 Etupes, France*

[c] *Femto-ST Institute (UMR CNRS 6174), Univ. Bourgogne Franche-Comté, UTMB, 2 Place Lucien Tharradin, 25200 Montbéliard Cedex, France*

[d] *Université Paris-Saclay, CEA, Service d'Etudes Analytiques et de Réactivité des Surfaces, 91191, Gif-sur-Yvette, France*

[e] *CEA Cross-cutting program on Materials and Processes Skills, 91191 Gif-sur-Yvette, France*

Abstract

High entropy alloy nitrides (AlCrTiV)N coatings were deposited by cathodic arc evaporation at various deposition bias and temperature. The mechanical properties of the as-deposited coatings and their oxidation resistance after annealing at various temperatures were analysed. X-ray analyses show in all coatings a FCC structure with a (111) preferred orientation up to 750°C. Up to 600°C, no oxygen penetration is measured in the films while at 800°C, critical spalling occurs for all samples. The coating deposited at a temperature of 300°C and negative bias of 100 V exhibits the most interesting compromise in both oxidation resistance and mechanical performances with a hardness of 40 GPa, a friction coefficient of 0.44 and a wear rate of $5.8 .10^{-7}$ $mm^3.N^{-1}.m^{-1}$. Annealing in air at 600°C for 2h reduces the wear rate to $2.1 .10^{-7}$ $mm^3.N^{-1}.m^{-1}$ and the surface hardness to 17 GPa. Although annealing forms a thin oxide layer that reduces the hardness on the surface of the coating, it also averages the hardness inside the film to 33 GPa regardless of the deposition bias.

Keywords: High-entropy alloys; Nitride coatings; Cathodic arc evaporation; Oxidation resistance; Mechanical properties

* Corresponding author.
E-mail addresses: matthieunussbaum@gmail.com, matthieu.nussbaum@dephis.com (M. Nussbaum)

Introduction

An important part of the research in the machining industry is focused on improving the lifetime of cutting tools. These tools are used in extreme conditions and need high wear resistance, oxidation resistance and excellent mechanical properties at high temperatures. Commercial nitrides like TiN, TiAlN or CrAlN [1] are often deposited on tungsten carbides to take advantage of their high hardness and high temperature properties [2] while some hard coatings are also multi- or nano-layered to enhance their properties [3].

In the last decade a new class of material, High Entropy Alloys (HEA), has seen a drastic increase in interest for many fields [4] from nuclear science [5] to medicine [6] as well as additive manufacturing [7], catalysis [8] and especially machining [9,10]. HEAs are made of multiple principal elements, each participating between 5 and 35 at.% of the composition [11,12]. The mixing of many principal elements with various properties increases the configurational entropy. High configurational entropy may lead to single-phase solid solutions, usually with a cubic nanocrystalline structure or amorphous. These multi-principal element systems often display distorted lattices with sluggish diffusion [13], cocktail effect [13,14] and interesting mechanical properties such as increased ductility [15–17], high hardness [15–18] and great resistance to wear [10,19] and oxidation [14,19]. Many studies show that the introduction of nitrogen into an HEA film increases its hardness and wear resistance even in extreme conditions to the point that some High Entropy Alloy Nitride (HEAN) coatings are proposed by reviewers as replacements for protective coatings like TiN, TiAlN or CrN in the machining industry [9,20,21].

Aluminium, titanium and chromium elements are extensively used in those compositions for their effects [22–25] on structure, strengthening and oxidation resistance of alloys. Vanadium is often used to improve the frictional and wear properties thanks to its atomic size deforming the crystal structure of both BCC and FCC alloys [3,26]. The metal AlCrTiV is

already studied for its mechanical properties as a lightweight alloy [27–29] and could be used in applications where the properties/cost ratio of compositions using hafnium or tantalum as strengthening elements [21,30,31] would be too high.

The properties of commercial nitride coatings are linked to the deposition process [32,33]. Inserts for machining are usually coated with Chemical Vapor Deposition (CVD) or Physical Vapor Deposition (PVD) processes [34]. Coatings deposited through the cathodic arc evaporation PVD process show great advantages such as high deposition rate [1,34,35], high ionization ratio [1,34,35] and the formation of stoichiometric nitride without closed loop control of the N_2 flow [21,36,37] compared to other conventional PVD methods such as Direct Current Magnetron Sputtering (DCMS) and High Power Impulse Magnetron Sputtering (HiPIMS). In this study, (AlCrTiV)N coatings are deposited through cathodic arc evaporation at different substrate temperature and bias voltage. The mechanical properties as well as the oxidation resistance of these coatings are investigated.

Experimental details

(AlCrTiV)N as HEAN coatings were deposited using a PLANAR cathodic arc evaporation system developed by Platit AG (Switzerland) with three arc targets (Ti, V and $Cr_{60}Al_{40}$) and a DC sputtering Al target. Because of the CrAl target composition and its low weight, Al tends to deposit less than the other elements by arc process on the substrate. Hence a DC sputtering target was used to compensate the deficit of Al from the arc target and obtain a quite equimolar composition. The coatings were deposited on mirror polished circular AISI M2 HSS (63 HRc, Ø 30 mm and 8 mm thick) samples and mirror polished 304L stainless steel flat coupons. Before deposition, all substrates were cleaned with ethanol and soap water then rinsed with clean water and dried. The substrates were fixed at 100 mm of the targets on a carousel turning at 7 rpm with double rotation. Their surfaces were first etched under 80 sccm

of Ar and 70 A of current applied on the Ti target while the substrate bias was fixed at -700 V. Then a Ti buffer layer about 0.17 ± 0.06 μm thick followed by an interlayer of TiN (~ 0.30 ± 0.06 μm) were deposited to enhance the adhesion of the HEAN coating. The HEANs films were deposited under a N_2 flow rate of 90 sccm with currents of 90, 60 and 90 A respectively applied on the Ti, V and $Cr_{60}Al_{40}$ arc targets for 90 minutes. Each target was powered by a separate Fronius DPS 2500 arc generator. The Al DC sputtering target was powered by a Solvix Magix 3kW pulsed-DC sputtering generator set at 2200 W in DC-mode. The substrate bias was controlled by a Solvix Magix 10 kW pulsed-DC bias generator. The deposition temperature, controlled by thermocouples on the two radiant heaters set opposite to each other on the walls of the reactor, varied between 200, 300 and 400°C and the negative substrate bias changed between 50, 100 and 150 V.

Although the bias voltage is always negative, the minus sign is not written to simplify notations and avoid confusions in the name of the samples. Each sample is named with "AlCrTiV" followed by its deposition bias voltage and temperature, e.g., AlCrTiV-50V-200C was-deposited with a 50 V negative bias voltage at 200°C.

The surfaces of the samples and their brittle fracture cross-sections were observed with a JEOL JSM-7800F field emission gun scanning electron microscope (FEG-SEM) at a working distance of 10 mm with either 15 or 5 kV of acceleration voltage and a scanning probe of 2 nA. The compositions were measured with a Bruker Quantax energy dispersive X-ray spectrometer (EDS). The structure of the samples was determined with a Bruker D8 X-ray diffractometer (XRD) in Bragg Brentano configuration with a Co source (λ_{Co} = 0.178897 nm) at a voltage of 35 kV and a current of 40 mA between the 2θ angles 20 and 110° with an increment step of 0.2° every 0.2 s.

Hardness and effective Young's modulus were measured with a CSM nanoindentation instrument (NHT). A Berkovich diamond tip was used as indenter at a loading and unloading

rate of 10 mN.min^{-1} to a maximum load of 20 mN. The penetration depth is lower than 10% of the coating thickness to exclude substrate influence [38]. The results are averaged using at least 10 measurements estimated with the Oliver and Pharr method [39]. The tribological properties were evaluated with a CSM ball-on-disc tribometer using a 6 mm diameter WC/Co ball as counter material at a constant load of 10 N sliding with a 3 mm radius circular movement for 30 000 laps (565 m) at 0.1 m.s^{-1}. The friction coefficient μ used is the average of the measures in the last 65 m (~3500 laps). The standard deviation between those measures is kept as error bars. All tests were performed at room temperature (~20°C) and relative humidity of about 40%. The wear track was investigated 4 times per sample with an Altisurf 500 profilometer equipped with an inductive probe to measure the mean wear volumes. The wear rate (W) is calculated with the equation $W = V_w / (L * S)$ using the mean wear volume (V_w), the normal load (L) and the sliding distance (S). The coating thickness was measured using a SCM Instruments Calotest with a 25 mm steel ball and a Leica DM 2400M optical microscope.

The samples were annealed in a Borel TL 1100-8 oven under air at different temperatures to test the oxidation resistance of the coatings. Each annealing temperature (from 400 to 800°C with a 50°C increment) was reached with a 100°C/h heating ramp and maintained for 2h. Samples are slowly cooled by turning off the heat and waiting for the closed oven to cool down to room temperature. After each annealing, the oxidation of the samples was investigated using XRD, SEM, EDS and a Horiba GD-OES (Glow Discharge Optical Emission Spectroscopy) analysis.

Results and discussion

Coatings composition and thickness

The atomic composition and thickness of each coating is presented in Figure 1. All nine (AlCrTiV)N samples are multi-element equiatomic compounds with about 50 ± 3 at.% nitrogen

and around 12.5 ± 1 at.% Al, Ti, V and Cr according to EDS measurements. The relative composition of metals (see Figure 1 (a)) shows that all samples are targeted composition. At all deposition temperatures, Al content slightly decreases as the bias voltage increases, which is attributed to preferential resputtering of Al.

The average thickness of the coatings presented in Figure 1 (b) is about 4.9 ± 0.4 µm. The deposition temperature does not seem to have a significant impact on the coating thickness between 200 and 300°C, but a slight increase in the film thickness is observed at 400°C. The coating thickness decreases with increasing bias voltage because of both densification and re-sputtering effects. A part of the energy used in both effects is dissipated as heat, increasing the film temperature. This may explain the difference in coating thickness between the AlCrTiV-100V-200C and 100V-300C samples as the importance of the energy contribution of the bias on the temperature rises with decreasing deposition temperature.

Film morphology and structure

X-ray diffraction patterns of the (AlCrTiV)N coatings are displayed in Figure 2 and show the influence during deposition of bias voltage on the samples deposited at 300°C in graph (a) and the influence of substrate temperature on the samples deposited at 100 V in graph (b). Four diffractograms are not displayed in this figure to ease the lecture of the graphs. The diffractogram of each sample can be found in the Supplementary data. All coatings share the same FCC structure with an intense peak at $2\theta \approx 43.6°$ corresponding to the (111) plans and two smaller peaks at 51 and 96° corresponding to the (200) and (222) plans, respectively. The smaller peak at 39.5° is an instrument detector anomaly related to the K_β radiation of the Co source, due to the high intensity peak at 43.6°.

In the diffractogram from Figure 2 (a), the relative intensity of the (111) plans increases with increasing negative deposition bias while the intensity of the (200) plans is unchanged.

This shows the importance of the deposition bias on the texture of the film [40]. Figure 2 (a') focuses on the (111) plans contribution and shows that an increase in deposition bias reduces the full width at half maximum (FWHM), indicating an increase in grain size. This grain growth is promoted by the heat generated from the incoming particles accelerated by the negative bias, raising the film temperature above the deposition temperature. The crystallite size calculated from the (111) peak of theses diffractograms using the Debye-Scherrer formula [41] seems to follow this trend with a grain size going from 24 ± 3 nm (50 V) to 34 ± 4 nm (100 V) and finally to 37 ± 4 nm (150 V).

A similar effect appears in Figure 2 (b'), although it is mostly visible at high temperatures, where an increase in deposition temperature induces a slight decrease in FWHM. As mentioned before, increasing the temperature of the sample increases atomic mobility, densifying the coating and leading to an increase in grain size [42]. According to calculations, this increase in grain size is not significant enough compared to our measurement error: 31 ± 4 nm (200C), 34 ± 4 nm (300C) and 33 ± 4 nm (400C). This confirms the observations of Chang *et al.* [42] on reactive DC magnetron sputtered (AlCrMoSiTi)N that the influence of substrate bias on grain size is greater than the influence of deposition temperature.

The lattice parameter is calculated from the (111) peak of Figure 2 (b') using Bragg's law [43] and the value is comprised within 4.16 ± 0.02 Å for all samples regardless of deposition temperature. A slight shift towards higher diffraction angles in Figure 2 (a') with increasing deposition bias are observed indicating the lattice parameter decrease. This decrease of the lattice parameter is due to the release of compressive stress in the film related to the heat generated by the incoming particles accelerated by the bias voltage.

Mechanical properties

The hardness and the Young's modulus of each sample are shown in Figure 3 (a) and (b) respectively. The surface of films deposited by arc evaporation is extremely rough because of the droplet effect. After polishing with a 2400-grade abrasive paper, the bigger droplets are removed but leave craters next to the smaller droplets, accounting for large error bars. The samples deposited at 400°C exhibit the lowest hardness values between 14 ± 4 and 22 ± 6 GPa. Coatings deposited at 300°C mostly displayed higher hardness than their counterparts. Maximum hardness values are achieved for 100 V bias. The increase in hardness from 50 V to 100 V is explained by the increase in compressive stress in the coating. The decline in hardness above 100 V follows our hypothesis that the residual compressive stress is reduced because of the heat generated by the increased bias voltage. However, the sample 150V-200C did not show any decline in hardness probably because the film temperature reached was not high enough to release the residual stress effectively. The maximum hardness was obtained for the sample deposited at 300°C and 100 V with 40 ± 6 GPa.

The Young's modulus of the coatings follows an evolution relatively similar to the hardness, with the lowest values for the films deposited at 400°C. Both Young's modulus and hardness decrease at 400°C. This effect could be explained by the relaxation of the compressive stress in the coating at higher temperatures. The H/E and H^3/E^2 ratios (presented in supplementary data) follow the same evolution as the graphs (a) and (b) from Figure 3.

The increase in bias voltage tends to densify the film and increase the compressive stress owing to the increasing average energy per impinging species. This is expected to increase the hardness, as can be seen with samples deposited at 200°C. But for the samples deposited at 300 and 400°C, a peak in hardness and modulus is attained at 100V of negative bias voltage. The slight decrease of hardness at 150V is ascribed to the heat generated by the accelerated particles at higher bias voltage that tends to relax some of the compressive stress. Similar results with a deposition at 100 V negative bias voltage inducing a peak in hardness were found by Chang *et*

al. [42] with the DC magnetron sputtering of (AlCrMoSiTi)N and Sobol et al. [36] with the vacuum-arc deposition of (AlCrTiZrNbV)N and (AlCrTiNbSi)N. The hardness of the sample 100V-300C is on par with the hardness of nitride coatings usually used for machining like TiN, TiAlN or CrAlN [3,44] that revolves around 35 GPa and the hardest HEANs of the literature that reach around 40 GPa [9,45]. Sobol *et al.* [36] managed to obtain a hardness of 55 GPa by vacuum-arc deposition of (HfTiZrNbV)N but Johansson *et al*. [46] reached at most 19 GPa with the same composition using reactive magnetron sputtering, showing the importance of deposition technology, especially through the ionization rate of the discharge.

Figure 3 (c) shows the influence of deposition temperature and bias voltage on the friction coefficient of the samples measured via a ball-on-disc tribological test. EDS mappings (presented in supplementary data) on all samples confirm the absence of substrate elements in the track. As shown by Figure 3 (c), the friction coefficient increases with increasing deposition temperature. The friction coefficient increases with the negative bias voltage up to 0.510 ± 0.004 for the films deposited at 400°C while, for the films deposited at 200 and 300°C, a slight decrease appears for the friction coefficient of the samples deposited with 100 V of bias voltage. The lowest value of friction coefficient is attained at 100 V for the film deposited at 200°C with 0.409 ± 0.005. The friction coefficient of HEANs in the literature varies between 0.15 [30] and 0.8 [21], depending on the composition. The experimental conditions of the tribological tests like the configuration (ball-on-disc, ball-on-plate…), the counterpart composition (Steel, WC/Co, Al_2O_3…) and the sliding speed, among others, vary greatly with each study. This highlights the need for standardised tests [47] to facilitate comparisons between coatings.

Figure 3 (d) represents the influence of the deposition temperature and bias voltage on the wear coefficient of the coating. Many parameters [47,48] besides hardness and friction coefficient influence the wear of a coating, like the surface roughness or the debris. The surface of arc deposited films is extremely rough, as shown in Figure 4, and difficult to differentiate

with the coating pushed back by the WC ball, hence the important error margins in Figure 3 (d). At a deposition temperature of 200°C, there seems to be no effect of the bias as the wear coefficient stays at its lowest value of 5.8 ± 0.8 10^{-7} $mm^3.N^{-1}.m^{-1}$. The samples deposited at higher temperatures show the highest wear coefficient of 8.8 ± 1.3 10^{-7} $mm^3.N^{-1}.m^{-1}$ when deposited at 50V of bias voltage. The lowest wear coefficient is also reached by all samples deposited with 100V of bias voltage regardless of the deposition temperature. A few HEANs in the literature reach wear rates as low as 2.3 10^{-7} $mm^3.N^{-1}.m^{-1}$ [49] or 3.23 10^{-7} $mm^3.N^{-1}.m^{-1}$ [50] by depositing (AlCrTiVZr)N through HiPIMS and (CrVTiNbZr)N through high ionization cathodic arc respectively. However, most HEANs display a wear rate in the 10^{-6} $mm^3.N^{-1}.m^{-1}$ order of magnitude [9,30] or higher [21].

Oxidation resistance

To study the evolution of the oxidation resistance of the films, the coatings deposited on M2 substrates were annealed for 2 h in air at different temperatures from 400 to 800°C. Up to 750°C, the surface oxide layer gradually increased with increasing temperature without any sign of coating deterioration while at 800°C all samples were completely oxidized and presented critical spalling.

XRD patterns were made after each annealing in air and are compiled in Figure 5 (a) for the 100V-300C sample. There is no significant change below 700°C in the crystalline structure for all deposition configurations compared to as-deposited patterns. The preferred orientation of all samples is the (111) direction up to 750°C. According to diffraction data[†], some oxides and nitrides based on Al, Ti, V or Cr and their combinations share similar structures with close diffraction peak angles to the observed FCC ones. Therefore, the contribution from the surface

[†] JCP 03-065-2899, 00-025-1495, 03-065-4307, 01-085-1381, 01-089-3660, 01-077-0047, 01-077-2173, among others.

oxides is not intense enough to be significantly differentiated from either the measurement noise or the HEAN pattern below annealing at 700°C.

After annealing at 700 and 750°C, new peaks start appearing at $2\theta = 32.1$ and 33.3° that could correspond to the (110) plans of TiO_2 (JCP 01-089-4920). After annealing at 800°C, the main FCC (111) peak at $2\theta = 44°$ and the small peak at 33.3° disappear while the peak 32.1° becomes the most intense with a twin at 32.7° that seem to correspond to the (111) plans of a mixed oxide like Al_2TiO_5 (01-070-1434) or $CrVO_4$ (00-015-0296).

After annealing at 800°C, the diffractograms of all samples are similar to those observed by Esmaily *et al.* [27] after annealing at 900°C for 24h of bulk AlCrTiV: peaks attributed to various oxides such as TiO_2, Al_2O_3 and V_2O_5 with some mixed oxides like $TiVO_4$.

Figure 6 shows GD-OES depth profiles compared with surface SEM observations of the 150V-200C sample after annealing at 600, 700 and 750°C. Oxygen rich crystallites grow on the surface with increasing temperature as shown by the inserts. The contribution of titanium at the interface between the film and the substrate around 3-3.5 µm relates to the pure Ti and TiN buffer layers. Passed this interlayer, the composition of the steel substrate is observed.

At 600°C, the nitrogen is depleted in the first 50 nm from the surface and replaced by oxygen. Similarly, the initial proportion of metallic elements shifts with a vanadium and aluminium enrichment of the oxidized area.

At 700°C, the oxygen diffuses up to 200 nm in depth from the surface. At 750°C, the oxygen diffusion accelerates and reaches about 900 nm in depth. Aluminium is present in higher proportions than the other alloying elements up to about 550 nm in depth. It seems the oxygen rich layer is divided in two parts: an outer layer made mainly of aluminium with varying amounts of Ti and V and an inner layer containing an excess of Cr before the transition into the HEAN film. The oxygen rich crystallites multiply to cover most of the surface. Two types of crystallites are visible on the SEM image in Figure 6. The faceted ones grow up to 1.2 ± 0.2

μm, according to measurements made with the ImageJ software, and they contain an excess of vanadium and aluminium according to EDS measurements. The needle and sheet-like ones grow up to a few microns in length and a hundred nanometres in depth and contain an excess in titanium and aluminium. At 800°C, macroscopic adhesive spallation occurs on all samples, including samples deposited on stainless steel substrates. GD-OES measurements are not presented but show an oxygen penetration from the surface of the film up to the substrate

Esmaily *et al.*'s study [27] shows that after 24h at both 700 and 900°C under air, the oxide layer is composed of oxides layers first rich in V, then rich in Ti, then Al and finally rich in Cr about 20 μm in depth from the surface. The GD-OES measurement made in the present study showed an excess of Al in the first 100 nm from the surface of the samples after all annealings below 800°C. The presence of other elements usually reduces the resistance to oxygen diffusion of a mixed aluminium oxide compared to pure alumina [51]. Therefore, the mixed oxides on the surface of the films are probably not a passivation layer but they are slowing down the oxygen penetration.

The same coatings, deposited on 304 stainless steel substrates, were annealed directly at 750°C for 2 hours in air to observe their oxidation resistance without the aging effect of successive annealing that may have formed the protective layer slowing the oxygen diffusion in the previously annealed samples. The ratios in percentages of oxygen penetration on the total thickness measured by GD-OES for each film after annealing are presented in Figure 7, as an alloy usually expands with the penetration of oxygen. For all deposition temperatures, an increase in deposition bias significantly increases the penetration of oxygen in the film after annealing and for all deposition bias, an increase in deposition temperature tends to reduce oxygen penetration. Both effects can be explained by a penetration of oxygen into the film through defects: incoming particles create more defects when they are accelerated by a higher

bias voltage while higher temperature favours the annihilation of defects with increased atomic mobility.

The sample 150V-200C displays an oxygen penetration of 77% of the film in Figure 7 while in Figure 6 it is equivalent to 22% of the film. This underlines the effect of the thermal treatments history of the film on its oxidation behaviour. Nevertheless, the operating temperature limit of 750°C is an improvement compared to TiN [44], often used on machining inserts, and some HEANs [9] as they are usually fully oxidised at 700°C though other standard machining coatings like CrAlN or TiAlN [44] and other HEANs [7] show great oxidation resistance at 900°C and above.

Mechanical properties after annealing at 600°C

(AlCrTiV)N films deposited at 300°C showed the most interesting combination of mechanical properties and oxidation resistance. The first oxygen rich layer appears on their surface at 600°C though oxygen barely penetrates the film, as shown in Figure 6. The mechanical properties of films annealed at 600°C for 2 hours in air, without previous thermal treatment, are shown in Figure 8 in dashed line (annealed in brown and polished after annealing in red) with the results of the as-deposited samples (plain lines) for reference.

According to Figure 8 (a), the maximum hardness value of 40 ± 6 GPa achieved by the as-deposited samples diminished to 17 ± 3 GPa after 2 hours at 600°C in air. This hardness is similar to that of TiN or CrN coatings after annealing at the same temperature for 1 hour [44]. The slight decrease in hardness with increasing deposition bias for the unpolished annealed samples is within measurement error but should result from a slightly thicker oxygen rich layer with increasing bias voltage. Furthermore, both H and E of the annealed samples are close to those of the samples as-deposited at 400°C, despite the relaxation of some of the compressive

stress in the coating and the important contribution of the surface oxygen rich crystallites that should be softer than the nitride beneath. The samples were polished with 1200-grade SiC paper until the surface oxygen rich crystallites were removed to measure the hardness in the bulk of the annealed coating without the contribution of the oxygen rich crystallites. Hardness of the polished annealed coatings reached 33 ± 3 GPa and E 500 ± 40 GPa, regardless of the deposition bias. Theses coatings hardness is almost double that of the commercial TiN and CrN coatings after annealing at 600°C [44]. The small decrease in hardness compared to the as-deposited sample at 100 V is probably a result of the relaxation of the compressive stress as EDS measurements show no significative variation in composition and the increase in calculated grain size in within measurement error. However, the increase in hardness for the samples deposited at 50 and 150 V shows that a different strengthening mechanism than residual stress is hardening the film. Higher temperatures favour grain growth and calculations show a tendency toward increased grain sizes within measurement error. The Hall-Petch effect usually shows strength peaks with grain sizes in the 20-30 nm range but it could be shifted toward the 30-60 nm range because of the atomic size differences in HEANs grains as it does for artifact-free nanocrystalline copper [52].

Figure 8 (c) shows that the friction coefficient μ is higher for annealed samples than as-deposited ones, except for the sample deposited at 150 V. Several studies show that the formation of oxides during wear tests tends to reduce wear as the oxides act as lubricant, especially vanadium oxides [3,53]. On the one hand, this effect may explain the decrease in friction coefficient. On the other hand, the surface oxygen rich crystallites lower the superficial hardness of the film which in turn is expected to increase the friction coefficient. In Figure 8 (d) the already low wear coefficient of the as-deposited samples at $5.8 \pm 0.2 \ .10^{-7}$ $mm^3.N^{-1}.m^{-1}$ is further reduced after annealing to $2.1 \pm 0.8 \ .10^{-7}$ $mm^3.N^{-1}.m^{-1}$.

However, an increase in friction coefficient is usually correlated with an increase in wear rate. The oxide debris on the harder coating beneath might have a peculiar effect on both the friction coefficient and the wear rate as they are probably softer than both the carbide ball and the nitride coating.

SEM images of the fracture cross-section from the samples annealed at 600°C are presented in Figure 9 and show that all coatings remain dense after annealing. The fracture of each coating is brittle.

The present paper dealt with equimolar AlTiCrV nitride. According to Hsieh *et al.*[54], who studied $(Al_{23.1}Cr_{30.8}Nb_{7.7}Si_{7.7}Ti_{30.7})_{50}N_{50}$ and $(Al_{29.1}Cr_{30.8}Nb_{11.2}Si_{7.7}Ti_{21.2})_{50}N_{50}$ films that displayed at most a 100 nm thin oxide layer after annealing in air for 2 h at 900°C, a higher Al and lower Ti content tend to increase the oxidation resistance of the film because of the superior oxygen diffusion inhibition of Al oxides [51] compared to rutile-TiO_2. Therefore, non-stoichiometric compositions of (AlCrTiV)N might further increase the properties of the HEAN, especially regarding high-temperature oxidation resistance.

Conclusion

(AlCrTiV)N HEANs coatings were prepared by cathodic arc evaporation and their mechanical properties and oxidation resistance were studied. XRD measurements revealed that the as-deposited FCC coatings have a (111) preferred orientation slightly promoted by the negative deposition bias voltage and the deposition temperature below 300°C. The mechanical properties of samples deposited at 400°C are degraded by the relaxation of the compressive stress in the coating. The film deposited at 100 V and 300°C shows the most promising mechanical properties with 40 and 583 GPa of hardness and Young's modulus respectively, a

friction coefficient of 0.44 and a wear coefficient of 5.8 $.10^{-7}$ $mm^3.N^{-1}.m^{-1}$. These mechanical properties are on par with the coatings used commercially on machining inserts or other HEANs and the wear rate is especially low. No oxygen penetration in the film was observed below 600°C as a thin Al-rich oxide protective layer forms on the surface of the films. The coatings show great mechanical properties even after annealing at 600°C for 2h in air with wear rate reduced further to 2.1 $.10^{-7}$ $mm^3.N^{-1}.m^{-1}$ while maintaining an acceptable hardness at 17 GPa on surface and a high hardness of 33 GPa in the bulk of the film. While critical oxidation and spalling occurs at 800°C, this coating may qualify for standard machining in future works.

Acknowledgement

This work was funded by the CEA-Saclay and the firm Dephis as members of the industrial research chair IMPACT. The authors are also indebted to the Pays de Montbéliard Agglomération (PMA) for its financial support.

References

[1] K.-D. Bouzakis, N. Michailidis, G. Skordaris, E. Bouzakis, D. Biermann, R. M'Saoubi, CIRP Ann. 61 (2012) 703–723.

[2] H.O. Pierson, in: H.O. Pierson (Ed.), Handb. Refract. Carbides Nitrides, William Andrew Publishing, Westwood, NJ, 1996, pp. 181–208.

[3] S. PalDey, S.C. Deevi, Mater. Sci. Eng. A 342 (2003) 58–79.

[4] D.B. Miracle, O.N. Senkov, Acta Mater. 122 (2017) 448–511.

[5] A. Kareer, J.C. Waite, B. Li, A. Couet, D.E.J. Armstrong, A.J. Wilkinson, J. Nucl. Mater. 526 (2019) 151744.

[6] K. Alagarsamy, A. Fortier, M. Komarasamy, N. Kumar, A. Mohammad, S. Banerjee, H.-C. Han, R.S. Mishra, Cardiovasc. Eng. Technol. 7 (2016) 448–454.

[7] J. Kim, A. Wakai, A. Moridi, J. Mater. Res. 35 (2020) 1963–1983.

[8] Y. Xin, S. Li, Y. Qian, W. Zhu, H. Yuan, P. Jiang, R. Guo, L. Wang, ACS Catal. 10 (2020) 11280–11306.

[9] A.D. Pogrebnjak, A.A. Bagdasaryan, I.V. Yakushchenko, V.M. Beresnev, Russ. Chem. Rev. 83 (2014) 1027–1061.

[10] S.A. Firstov, V.F. Gorban', N.A. Krapivka, M.V. Karpets, A.D. Kostenko, Powder Metall. Met. Ceram. 56 (2017) 158–164.

[11] B. Cantor, K.B. Kim, P.J. Warren, J. Metastable Nanocrystalline Mater. 13 (2002) 27–32.

[12] J.-W. Yeh, S.-K. Chen, S.-J. Lin, J.-Y. Gan, T.-S. Chin, T.-T. Shun, C.-H. Tsau, S.-Y. Chang, Adv. Eng. Mater. 6 (2004) 299–303.

[13] J.-W. Yeh, Ann. Chim. Sci. Matér. 31 (2006) 633–648.

[14] J. Chen, X. Zhou, W. Wang, B. Liu, Y. Lv, W. Yang, D. Xu, Y. Liu, J. Alloys Compd. 760 (2018) 15–30.

[15] M. Mroz, Design and Structural Optimization of a High Entropy Alloy (HEA) of the CoCrFeMnNi Family with High Mechanical Resistance., Université de Lyon, 2018.

[16] R.K. Nutor, Q. Cao, X. Wang, D. Zhang, Y. Fang, Y. Zhang, J.-Z. Jiang, Adv. Eng. Mater. 22 (2020) 2000466.

[17] I. Baker, Metals 10 (2020) 695.

[18] A.O. Soto, A.S. Salgado, E.B. Niño, Intermetallics 124 (2020) 106850.

[19] P.-K. Huang, J.-W. Yeh, T.-T. Shun, S.-K. Chen, Adv. Eng. Mater. 6 (2004) 74–78.

[20] C.-H. Chang, C.-B. Yang, C.-C. Sung, C.-Y. Hsu, Thin Solid Films 668 (2018) 63–68.

[21] S.N. Grigoriev, O.V. Sobol, V.M. Beresnev, I.V. Serdyuk, A.D. Pogrebnyak, D.A. Kolesnikov, U.S. Nemchenko, J. Frict. Wear 35 (2014) 359–364.

[22] T. Cao, J. Shang, J. Zhao, C. Cheng, R. Wang, H. Wang, Mater. Lett. 164 (2016) 344–347.

[23] C.-C. Tung, J.-W. Yeh, T. Shun, S.-K. Chen, Y.-S. Huang, H.-C. Chen, Mater. Lett. 61 (2007) 1–5.

[24] Z.D. Han, N. Chen, S.F. Zhao, L.W. Fan, G.N. Yang, Y. Shao, K.F. Yao, Intermetallics 84 (2017) 153–157.

[25] D. Ikeuchi, D.J.M. King, K.J. Laws, A.J. Knowles, R.D. Aughterson, G.R. Lumpkin, E.G. Obbard, Scr. Mater. 158 (2019) 141–145.

[26] B. Yin, F. Maresca, W.A. Curtin, Acta Mater. 188 (2020) 486–491.

[27] M. Esmaily, Y. Qiu, S. Bigdeli, M.B. Venkataraman, A. Allanore, N. Birbilis, Npj Mater. Degrad. 4 (2020) 25.

[28] D. Li, Y. Dong, Z. Zhang, Q. Zhang, S. Chen, N. Jia, H. Wang, B. Wang, K. Jin, Y. Xue, Y. Dou, X. He, W. Yang, L. Wang, H. Cai, J. Alloys Compd. (2021) 160199.

[29] X. Huang, J. Miao, A.A. Luo, J. Mater. Sci. 54 (2019) 2271–2277.

[30] V. Braic, A. Vladescu, M. Balaceanu, C.R. Luculescu, M. Braic, Surf. Coat. Technol. 211 (2012) 117–121.

[31] O.N. Senkov, J.M. Scott, S.V. Senkova, D.B. Miracle, C.F. Woodward, J. Alloys Compd. 509 (2011) 6043–6048.

[32] J.-E. Sundgren, Thin Solid Films 128 (1985) 21–44.

[33] J. -E. Sundgren, H.T.G. Hentzell, J. Vac. Sci. Technol. Vac. Surf. Films 4 (1986) 2259–2279.

[34] Y. Deng, W. Chen, B. Li, C. Wang, T. Kuang, Y. Li, Ceram. Int. 46 (2020) 18373–18390.

[35] B. Engers, H. Fuchs, J. Schultz, E. Hettkamp, H. Mecke, Surf. Coat. Technol. 133–134 (2000) 121–125.

[36] O.V. Sobol', A.A. Andreev, V.F. Gorban', H.O. Postelnyk, V.A. Stolbovoy, A.V. Zvyagolsky, A.V. Dolomanov, Z.V. Kraievska, Past (2019) 127–135.

[37] R. Krause-Rehberg, A.D. Pogrebnyak, V.N. Borisyuk, M.V. Kaverin, A.G. Ponomarev, M.A. Bilokur, K. Oyoshi, Y. Takeda, V.M. Beresnev, O.V. Sobol', Phys. Met. Metallogr. 114 (2013) 672–680.

[38] H. Bückle, Metall. Rev. 4 (1959) 49–100.

[39] W.C. Oliver, G.M. Pharr, J. Mater. Res. 7 (1992) 1564–1583.

[40] Y. Zhang, P. YAN, Z. WU, P. ZHANG, Rare Met. 24 (2005) 370.

[41] A.L. Patterson, Phys. Rev. 56 (1939) 978–982.

[42] H.-W. Chang, P.-K. Huang, J.-W. Yeh, A. Davison, C.-H. Tsau, C.-C. Yang, Surf. Coat. Technol. 202 (2008) 3360–3366.

[43] H.G.J. Moseley, Lond. Edinb. Dublin Philos. Mag. J. Sci. 26 (1913) 1024–1034.

[44] Y.C. Chim, X.Z. Ding, X.T. Zeng, S. Zhang, Thin Solid Films 517 (2009) 4845–4849.

[45] P.-K. Huang, J.-W. Yeh, Thin Solid Films 518 (2009) 180–184.

[46] K. Johansson, L. Riekehr, S. Fritze, E. Lewin, Surf. Coat. Technol. 349 (2018) 529–539.

[47] A. Matthews, A. Leyland, K. Holmberg, H. Ronkainen, Surf. Coat. Technol. 100–101 (1998) 1–6.

[48] K. Holmberg, A. Matthews, Thin Solid Films 253 (1994) 173–178.

[49] Y. Xu, G. Li, Y. Xia, Appl. Surf. Sci. 523 (2020) 146529.

[50] Y.-Y. Chang, C.-H. Chung, Coatings 11 (2021) 41.

[51] C.-H. Chang, M.S. Titus, J.-W. Yeh, Adv. Eng. Mater. 20 (2018) 1700948.

[52] S.H. Whang, in: Nanostructured Met. Alloys, Elsevier, 2011, pp. xxi–xxxv.

[53] W. Tillmann, D. Kokalj, D. Stangier, M. Paulus, C. Sternemann, M. Tolan, Surf. Coat. Technol. 328 (2017) 172–181.

[54] M.-H. Hsieh, M.-H. Tsai, W.-J. Shen, J.-W. Yeh, Surf. Coat. Technol. 221 (2013) 118–123.

List of figure captions

Figure 1: (a) HEAN thin film composition (in at. % ± 1 %) measured by EDS and (b) film thickness vs deposition conditions: bias voltage (V) and substrate temperature (°C).

Figure 2: XRD patterns showing influence of the deposition conditions (a) negative bias voltage and (b) substrate temperature on the FCC structure of the (CrAlTiV)N coatings deposited on M2 substrates.

Figure 3: Influence of deposition bias voltage and substrate temperature on the (a) hardness H and (b) Young modulus E measured by nano-indentation and the (c) friction and (d) wear coefficients measured by tribological tests of (CrAlTiV)N films deposited on M2 substrates

Figure 4: Example of a measurement of the wear track with the tribometer on the 100V-300C sample after the tribological test.

Figure 5: XRD patterns of the sample 100V-300C after each annealing with patterns shifted vertically in decreasing annealing temperature from top to bottom

Figure 6: (left) Atomic composition in depth measured by GD-OES and (right) SEM images of the surface of the sample 150V-200C after annealing at 600, 700 and 750°C

Figure 7: Influence of deposition temperature and bias on the film oxidation after annealing at 750°C for 2 hours in air. Film oxidation is the ratio of the thickness of the oxidized film on the total thickness of the film measured by GD-OES.

Figure 8: Influence of annealing for 2h in air at 600°C for the (CrAlTiV)N films deposited at 300°C (brown dashed lines) compared to as-deposited samples (plain lines) on (a) hardness H, (b) Young's modulus E, (c) friction coefficient and (d) wear coefficients. H and E were also measured after polishing the surface of the samples to remove the oxides (red dashed lines).

Figure 9: SEM images of the brittle fracture cross-section made from the samples deposited at 300°C after annealing at 600°C in air for 2h.

List of figures

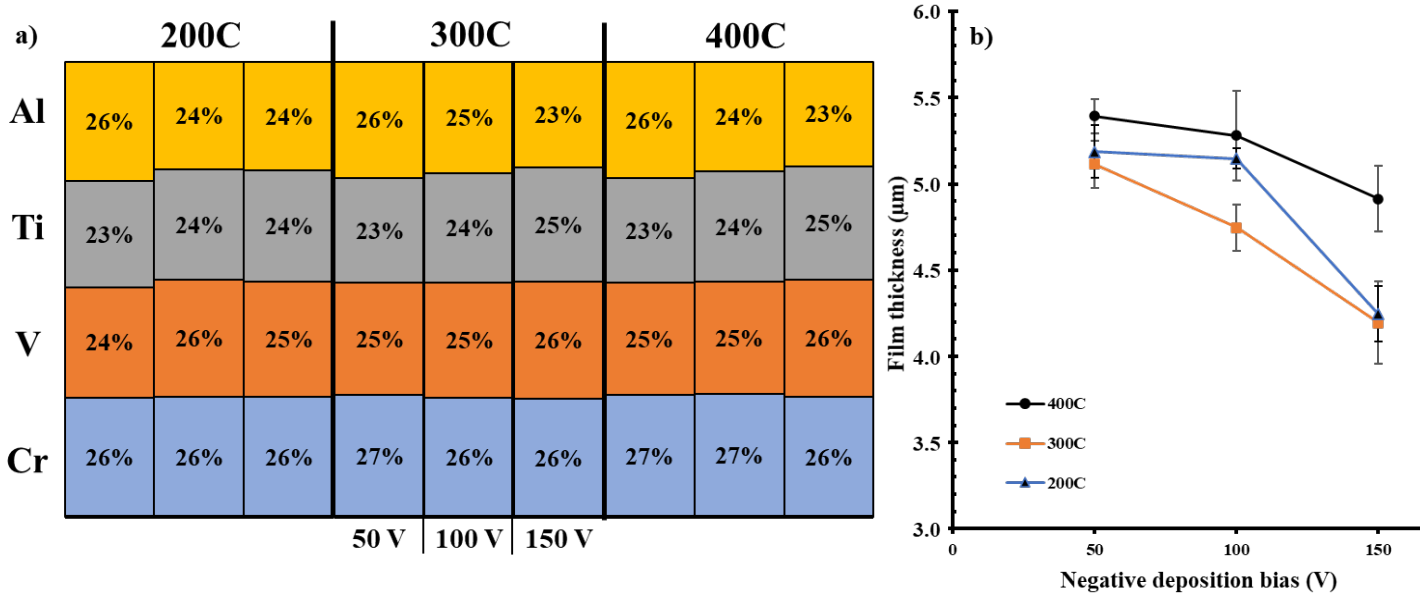

1

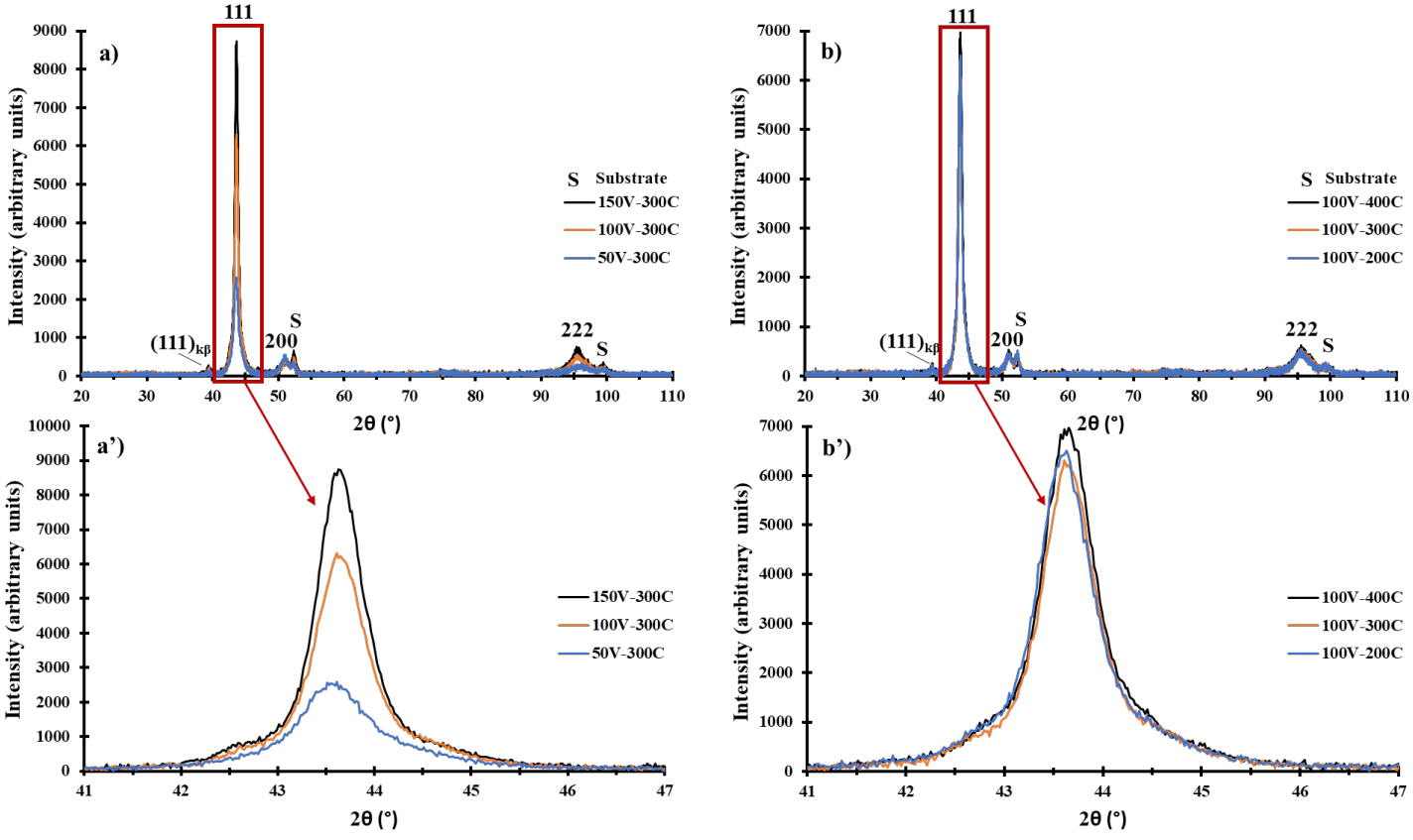

2

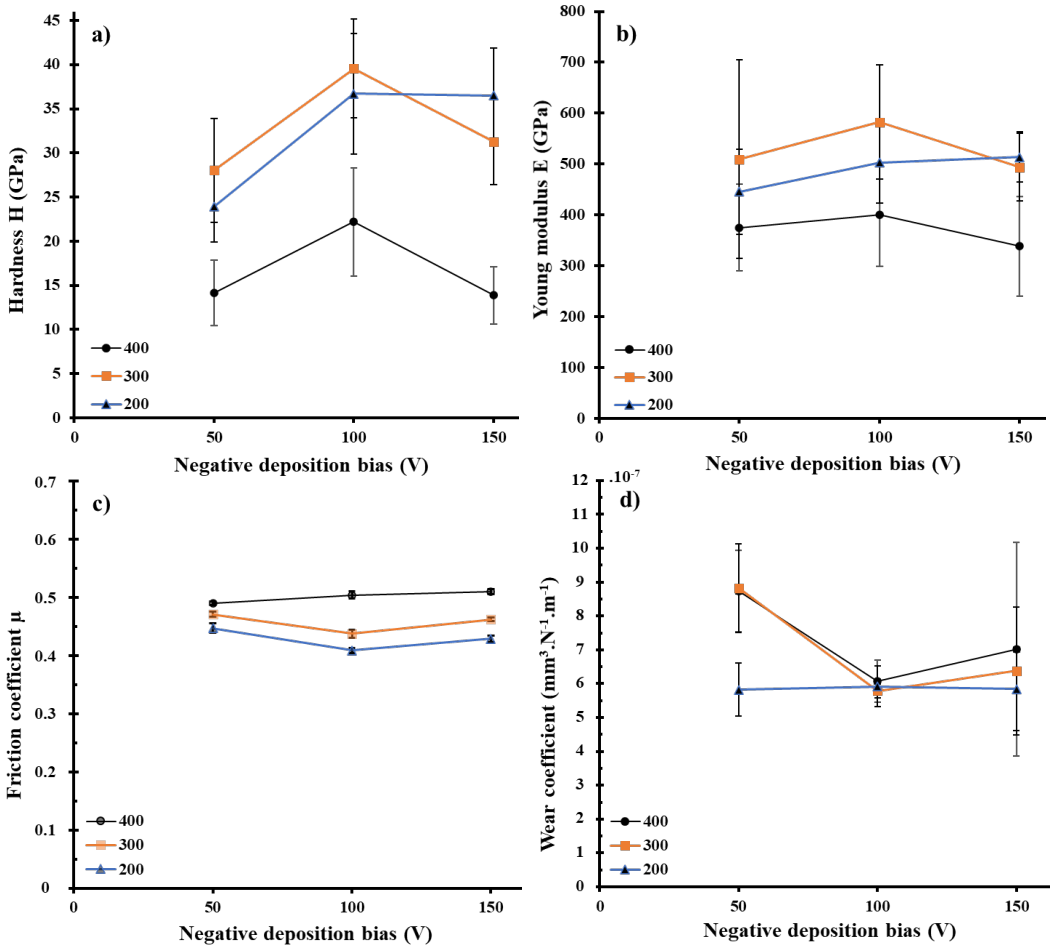
a)
Hardness H (GPa)
Negative deposition bias (V)
400
300
200
b)
Young modulus E (GPa)
Negative deposition bias (V)
c)
Friction coefficient μ
Negative deposition bias (V)
d)
.10-7
Wear coefficient (mm3.N-1.m-1)
Negative deposition bias (V)

3

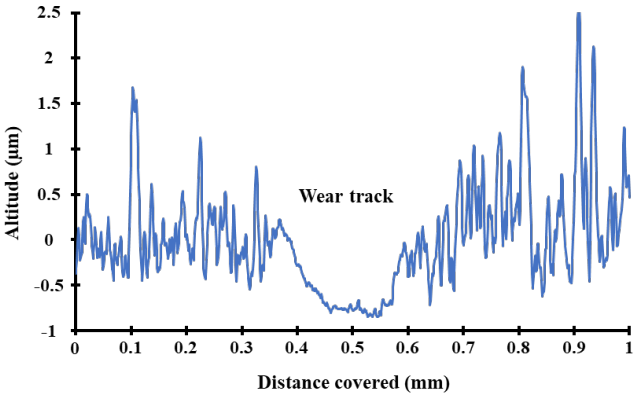
Altitude (μm)
Wear track
Distance covered (mm)

4

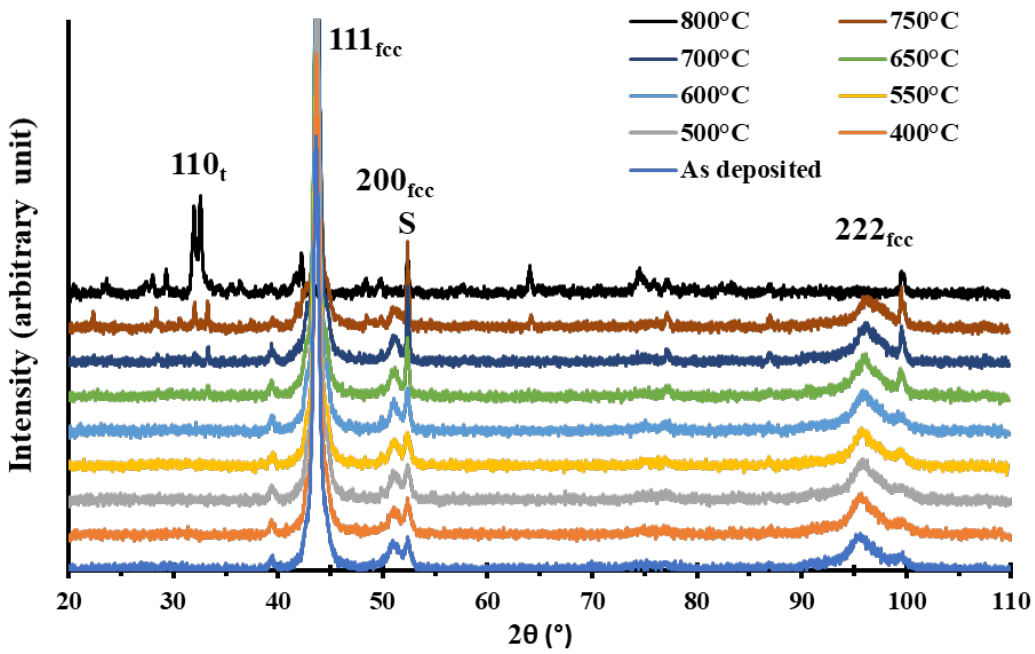
800°C
750°C
700°C
650°C
600°C
550°C
500°C
400°C
As deposited
111fcc
110t
200fcc
S
222fcc
Intensity (arbitrary unit)
20
30
40
50
60
70
80
90
100
110
2θ (°)

5

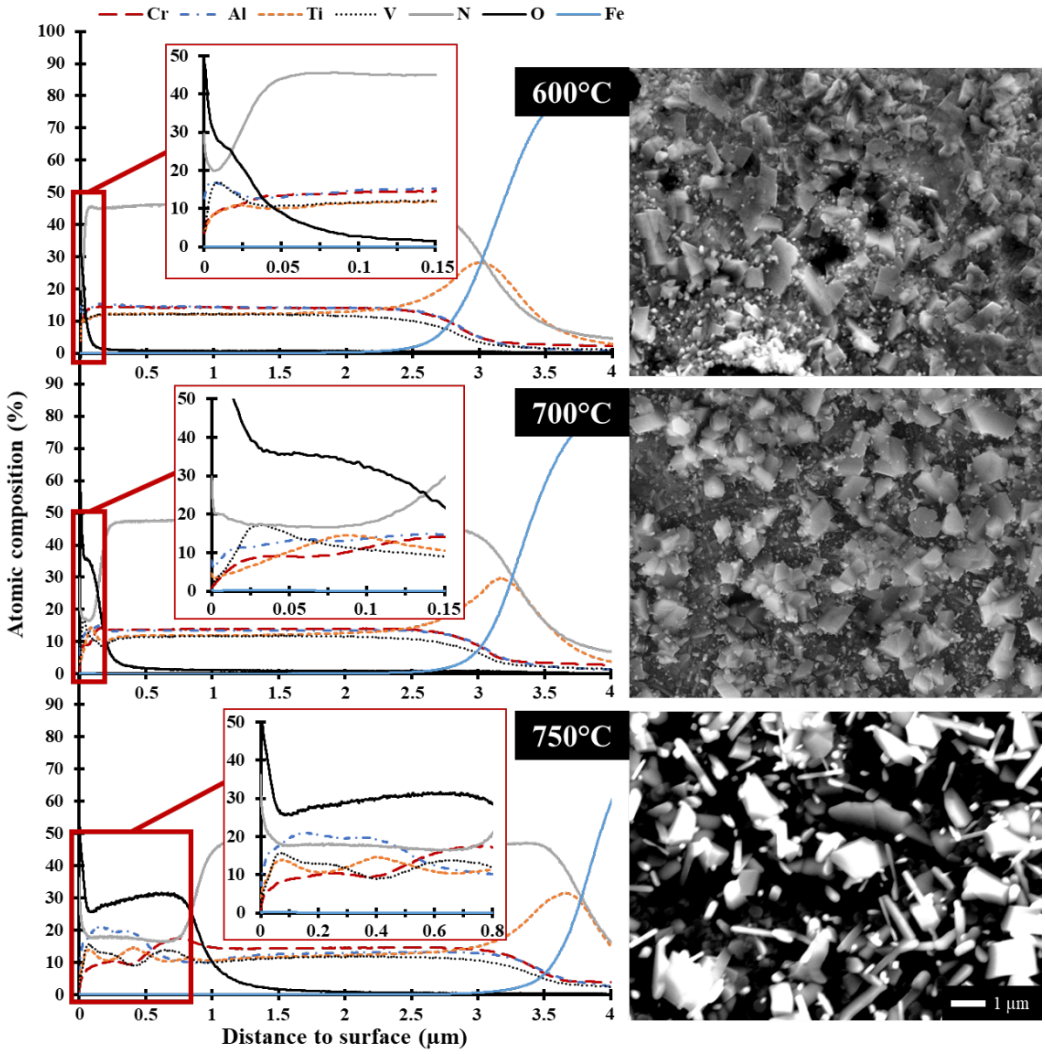
Cr
Al
Ti
V
N
O
Fe
600°C
700°C
750°C
1 µm
Atomic composition (%)
Distance to surface (µm)

6

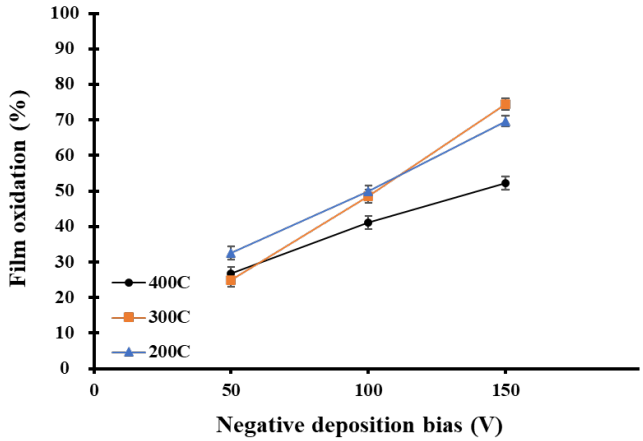
Film oxidation (%)
Negative deposition bias (V)
400C
300C
200C

7

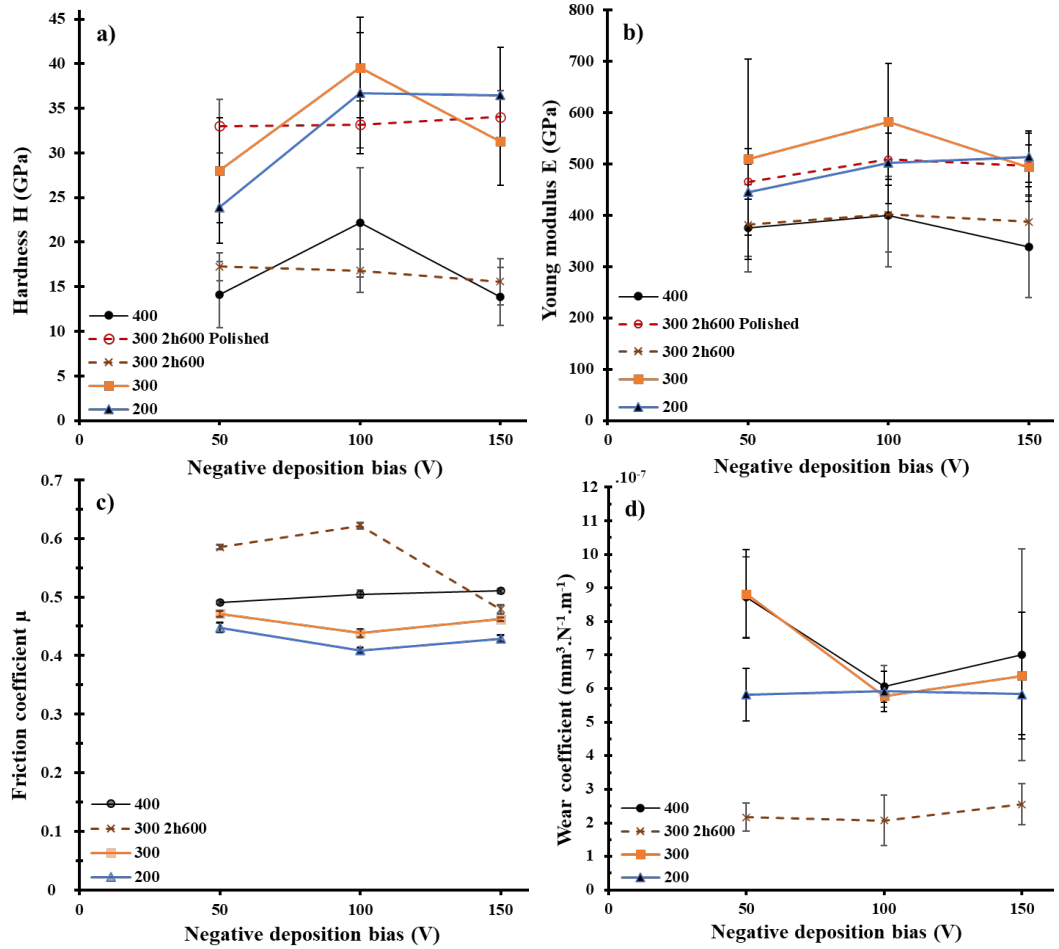
a)
Hardness H (GPa)
Negative deposition bias (V)
400
300 2h600 Polished
300 2h600
300
200
b)
Young modulus E (GPa)
Negative deposition bias (V)
c)
Friction coefficient μ
Negative deposition bias (V)
d)
.10-7
Wear coefficient (mm3.N-1.m-1)
Negative deposition bias (V)

8

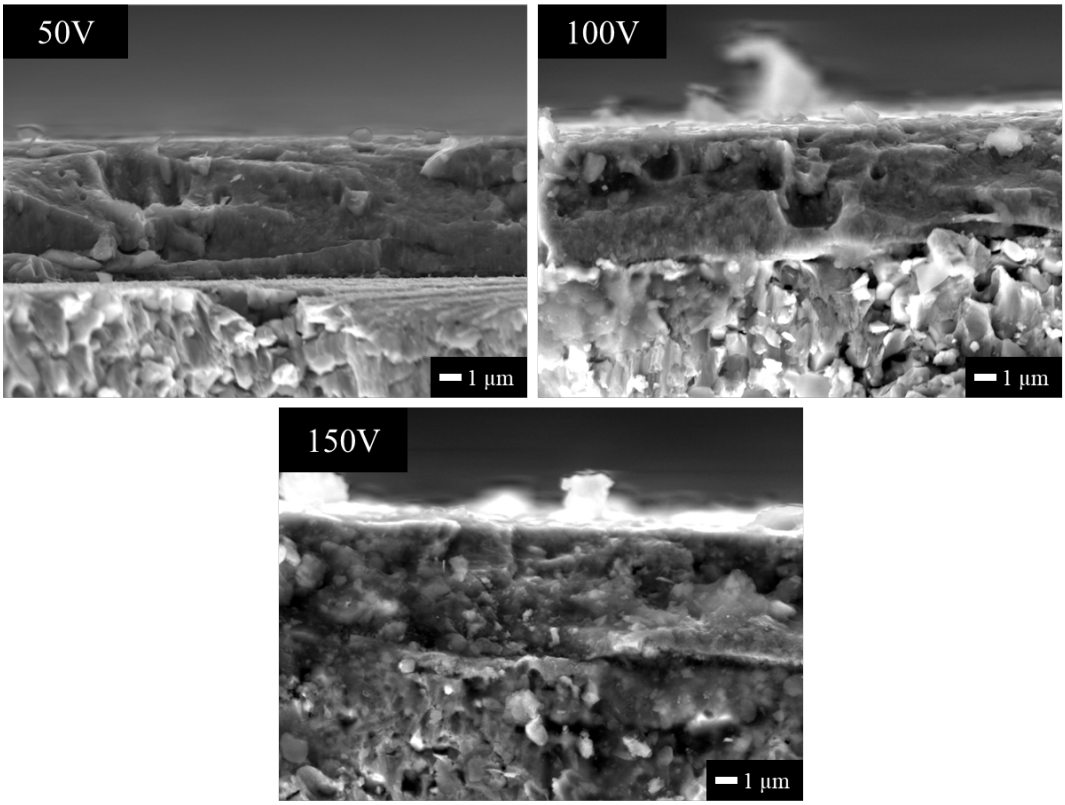
50V
1 µm
100V
1 µm
150V
1 µm